# Electron correlations in atomic valence shells: Magnesium and aluminum

Patrick F. O'Mahony*
*Department of Physics, University of Chicago, Chicago, Illinois 60637*
(Received 18 December 1984)

We use a combination of $R$-matrix and hyperspherical coordinate techniques to study the effects of electron correlations in atomic valence shells. The $3snd$-$3p^2$ mixing in Mg $^1D^e$ is analyzed in detail and its relevance to the $s^2p^nd$-$sp^{n+2}$ interactions throughout the row is indicated by a study of the $3s^2nd$-$3s\,3p^2\,^2D^e$ mixing in Al. Multichannel quantum-defect theory parameters for Mg $^1D^e$ and Al $^2D^e$ are calculated *ab initio*. We obtain excellent agreement with experiment for the quantum defects of the $3snd$ series in Mg and a significant improvement over previous theoretical studies for the quantum defects of the $3s^2nd$ series in Al. Two-electron correlations are illustrated by mapping their joint probability density for alternative eigenmodes.

## I. INTRODUCTION

The simultaneous excitation of two electrons from an atomic valence shell can have a major effect on the spectrum of that atom. This is particularly true for open-shell atoms where the energy required for double excitation is often smaller than the ionization energy. Open-shell atoms may therefore have doubly excited states quasidegenerate with a Rydberg series of the same symmetry. As a result, in the language of configuration mixing, the eigenfunctions of a whole Rydberg series of levels and its adjoining continuum contain major and varying admixtures of one or more doubly excited configurations. A well-known example of this type is the $^2D^e$ principal series of aluminum.[1,2]

Photoexcitation of Al I from its ground state $3s^23p\,^2P^o$ leads to either $3s^2nd\,^2D^e$ or $3s^2ns\,^2S^e$ by dipole selection rules. It has been observed experimentally, and illustrated by Lin[1] through a semiempirical quantum-defect analysis, that the oscillator strength of the $3s\,3p^2\,^2D^e$ configuration is distributed throughout the $3s^2nd$ Rydberg series and into the $3s^2\epsilon d$ continuum. No particular energy level can be associated with the $3s\,3p^2$ configuration. An initial calculation by configuration interaction (CI) including the lowest members of the $3s^2nd$ series and the $3s\,3p^2$ configuration raised the $3s\,3p^2$ level, located in the Hartree-Fock approximation between the $3s^25d$ and $3s^26d$ levels, all the way into the $3s^2\epsilon d$ continuum.[3] Such CI-type calculations have since been modified to include effects due to the continuum, although in a somewhat artificial manner by including pseudoorbitals which oscillate like continuum orbitals within the valence-shell radius but are bound orbitals nonetheless.[4]

The $3s\,3p^2\,^2S^e$, on the other hand, fails to perturb the $3s^2ns\,^2S^e$ levels to any great extent, it being a well-defined autoionizing state located just above the $Al^+\ ^1S^e$ threshold.[5] This difference between the $^2S^e$ and the $^2D^e$, completely governed by the short-range dynamics, brings out the need to view the interactions of a series of doubly excited states and a Rydberg series of levels as the interaction between different channels as opposed to a level-by-level analysis. (A channel is defined as consisting of all the configurations that differ only by an $n$ quantum number, e.g., $3s^2ns$ and $3s^2\epsilon s$.)

Channel mixing has been seen to proceed through localized avoided crossings between adiabatic potential curves in hyperspherical coordinates[6]—a concept familiar in atom-atom collisions at low energy where excitation occurs through nonadiabatic transitions between Born-Oppenheimer potential curves. A recent analysis has shown that crossings of adiabatic potential curves will occur systematically due to the fact that angular excitation is energetically favored over radial excitation in the "condensation region," where all the electrons are close to the nucleus.[7] The reverse, however, occurs when one electron escapes to a large radius, thus leading to curve crossings at some intermediate radius. The detailed circumstances which govern these crossings remain to be investigated.

This paper extends the main techniques of theoretical spectroscopy, i.e., CI, multiconfiguration Hartree-Fock by demonstrating that the mechanics of a many-electron atom can be understood by analyzing its eigenfunctions in their configuration space. This analysis may in fact be essential in order to classify spectroscopically a Rydberg series of levels, the independent-particle quantum numbers proving wholly inadequate in many cases.

The analysis of the spectrum of the doubly excited states of helium has already demonstrated this to be the case for a two-electron atom. An early study by Cooper, Fano, and Prats[8] showed that the $^1P^o$ spectrum of the doubly excited states of helium converging to the $He^+(N=2)$ threshold can be approximately represented by the superpositions $2snp \pm 2pns$, the so-called plus or minus states. More recently Lin, in a hyperspherical treatment of the doubly excited states of helium converging to the $He^+(N=3)$ threshold, has introduced a set of approximate quantum numbers to replace the conventional set $(n_1l_1)(n_2l_2)^{2S+1}L^\pi$, namely, $\{n,N,(K,T)^A,L,S,\pi\}$, which describe both radial and angular correlations.[9] The $K$ and $T$ quantum numbers were first introduced by Herrick and Sinanoğlu to describe intrashell correlations in helium.[10] Lin has reinterpreted them, $K$ and $T$ now being used to describe angular correlations only, while

 

$A=+1$, $-1$, or 0 label the radial correlations, $A=\pm 1$ corresponding to the $\pm$ designation of Cooper *et al.* and $A=0$ describing correlation patterns characteristic of singly excited states. This scheme enables one to group energy levels having identical $(K,T)^A$ but different $L,S,\pi$ into a supermultiplet structure,[11] a classification scheme totally foreign to traditional spectroscopy.

The relevance of these studies of helium to the more accessible spectra of the alkaline earths was made clear by Greene in his hyperspherical study of the $^1P^o$ states of beryllium[12] (see also O'Mahony and Greene[13]). He showed that eigenmodes of the $^1P^o$ states exhibit the same plus-and-minus-type character as in helium despite the fact that the $Be^+$ $2s$ and $2p$ levels are not degenerate as they are in helium. Further investigations on the Mg I $^1P^o$ states have reinforced his conclusions,[13] but much work remains to be done on the heavier alkaline earths and on different $\{L,S,\pi\}$ states to understand the effects of electron correlations in these atoms.

The above progress hinged on the analysis of wave functions in configuration space. In this paper we extend these studies to the type of gross perturbation of a Rydberg series mentioned earlier with respect to aluminum. As an initial step we examine channel interaction in the $^1D^e$ states of magnesium where the "$sd$" and "$p^2$" channels will be seen to mix strongly. This is the prototype for the $s^2p^nd-sp^{n+2}$ interaction along whole rows of the Periodic Table. For example, in Al I one of the $s$ electrons can be thought of as a "spectator," i.e., by recoupling the matrix element

$$\langle 3s^2nd\,^2D^e \left| \left[\sum_{i>j} 1/r_{ij}\right] \right| 3s3p^2\,^2D^e\rangle$$

into the form

$$\langle [(3s)^2S^e(3snd)^1D^e]^2D^e \left| \left[\sum_{i>j} 1/r_{ij}\right] \right. \times \left| [(3s)^2S^e(3p^2)^1D^e]^2D^e\right\rangle .$$

This interaction dominates the principal series of all the elements in the same row. In fact, a semiempirical quantum-defect analysis of the $3s3p^3\,^3P^o$ mixing in the $3s^23pnd\,^3P^o$ series of silicon was the motivating force behind the present study.

We shall use a combination of hyperspherical and $R$-matrix techniques, already illustrated in a previous paper,[14] to analyze the dynamics of channel interactions and to provide reliable spectroscopic data. The *ab initio* calculation of multichannel quantum-defect theory (MQDT) parameters is an integral part of this analysis.[15] Quantum defects of discrete levels and phase shifts in the autoionization region are calculated from a small set of MQDT parameters.[16] A full description of electron correlations in the $^1D^e$ spectrum of magnesium is provided through plots of the probability density in configuration space. Quantum defects for Al I are calculated and an outline of the dynamics of three electrons outside a closed shell is given. Eludication of the mechanics of a three-electron system is in its infancy due to the large number of variables involved. However reconstruction of the dynamics should be possible by plotting different sections of the probability density in configuration space. Preliminary investigations in this direction have been carried out[17,18] but much remains for future study, together with extensions to groups IV–VII.

The division of space into distinct regions where different forces dominate and the subsequent analysis of the solutions in each of these regions plays a central role in this paper both in implementing a calculational scheme and in understanding the solutions. In particular, we separate the volume in space where all the electrons interact strongly from that region where one electron escapes this volume to large distances, moving in a Coulomb or some other appropriate long-range field. The electron's motion in a long-range field can be treated in general analytically of semianalytically as for single-electron excitations.

Section II describes the results obtained for Mg I $^1D^e$, Sec. III presents the results for Al I, and Sec. IV gives a discussion of the results and an analysis of future directions.

## II. MAGNESIUM $^1D^e$

### A. Outline of the hyperspherical method

The Schrödinger equation for two electrons outside a closed-shell core can be written, in atomic units, as follows:

$$H\psi=\left[-\tfrac{1}{2}\nabla_1^2-\tfrac{1}{2}\nabla_2^2+V(r_1)+V(r_2)+\frac{1}{r_{12}}\right]\psi=E\psi\ , \tag{1}$$

where the interaction of each valence electron with the closed-shell core is represented by a local potential $V(r)$. [We use Hartree-Slater potentials for $V(r)$ throughout this paper.[19]] There have been many approaches to the solution of Eq. (1) over a limited energy range. We present initially the hyperspherical coordinate approach.[20]

One replaces the independent electron coordinates $r_1$ and $r_2$ by

$$R=(r_1^2+r_2^2)^{1/2}\ ,\quad \alpha=\tan^{-1}\left[\frac{r_2}{r_1}\right]\ , \tag{2}$$

$R$ being a measure of the "size" of the system and $\alpha$ serving as a radial correlation coordinate. Equation (1) then becomes,[20] in terms of $R$ and $\alpha$, on substituting,

$$r_1=R\cos\alpha\ ,\quad r_2=R\sin\alpha\ , \tag{3}$$

$$\left[\frac{\partial^2}{\partial R^2}+\frac{1}{4R^2}+(E-\hat{U})\right]\psi=0\ , \tag{4}$$

where

$$\hat{U}(R;\Omega)=\frac{1}{R^2}\left[-\frac{1}{2}\frac{\partial^2}{\partial\alpha^2}+\frac{l_1^2}{2\cos^2\alpha}+\frac{l_2^2}{2\sin^2\alpha}+V(R\cos\alpha)+V(R\sin\alpha)+\frac{1}{r_{12}}\right]\ , \tag{5}$$

$l_1^2$ and $l_2^2$ are the orbital angular momenta of the two elec-

trons, and $\Omega=\{\alpha,\theta_1,\phi_1,\theta_2,\phi_2\}$ represents the angular variables. We solve Eq. (4) in the adiabatic approximation at each value of $R$, which is equivalent to finding the eigenvalues of the operator $\hat{U}$,

$$\hat{U}(R;\Omega)\Phi_\mu(R;\Omega)=U_\mu(R)\Phi_\mu(R;\Omega)\ . \tag{6}$$

The adiabatic eigenfunctions $\Phi_\mu(R;\Omega)$ contain information on both radial and angular correlations as functions of $R$ whereas the $U_\mu(R)$ serve as effective potentials for the motion in $R$. Nonadiabatic effects due to the derivatives in $R$ in Eq. (4) can be taken into account if necessary in the complete solution, by expanding the total wave function in terms of the adiabatic solutions, $\psi=\sum_\mu F_\mu(R)\Phi_\mu(R;\Omega)$. A set of coupled equations for $F_\mu(R)$ is obtained on substitution in (4). For a pair of electrons, Eq. (6) is solved by expanding $\Phi(R;\Omega)$ in a basis set of antisymmetric wave functions coupled to a given total orbital angular momentum **L** and spin **S**,

$$\Phi(R;\Omega)=A\sum_{n_1l_1n_2l_2} C^{l_1l_2}_{n_1n_2}G_{n_1l_1}(r_1)F_{n_2l_2}(r_2)\times Y_{l_1l_2LM}(\theta_1,\phi_2,\theta_2,\phi_2)\times[\chi_{s_1m_1}(1)\chi_{s_2m_2}(2)]^S\ , \tag{7}$$

where $A$ denotes antisymmetrization. Using suitably chosen Slater orbitals for $G_{n_1l_1}(r_1)$ and $F_{n_2l_2}(r_1)$ and substituting for $r_1$ and $r_2$ in terms of $R$ and $\alpha$ as in Eq. (3), we can write (7) explicitly in terms of the set of variables $R$ and $\alpha$.[21] Subsequent substitution of (7) in (6) and diagonalization at each fixed value of $R$ yields the eigenvalues $U_\mu(R)$ and the adiabatic functions $\Phi_\mu(R;\Omega)$.

### B. $^1D^e$ potential curves and adiabatic functions

The $3s\epsilon d$ and $3p\epsilon p$ are the channels of interest for the magnesium $^1D^e$. $3pnf\,^1D^e$ channel interacts weakly with these channels, the large angular momentum of the $f$ electron keeping it out of the interaction region. Therefore the sum in Eq. (7) contains only the $(l_1,l_2)$ pairs (0,2) and (1,1). The potential curves are calculated as described in Sec. II A and are shown in Fig. 1. $U_1(R)$ converges to the $Mg^+(3s)$ threshold and $U_2(R)$ goes to the $Mg^+(3p)$ level at large $R$. The two curves $U_1$ and $U_2$ have a strongly avoided crossing at $R\approx 6.5$ a.u. The effects of this crossing will be discussed later.

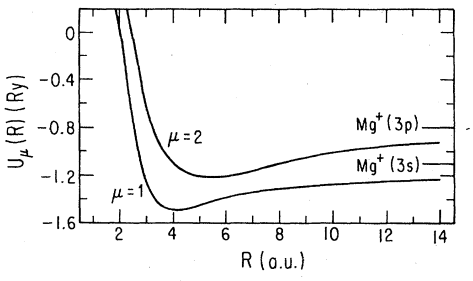


FIG. 1. Two lowest Mg $^1D^e$ adiabatic potential curves $U_\mu(R)$ plotted as functions of the radius $R$.

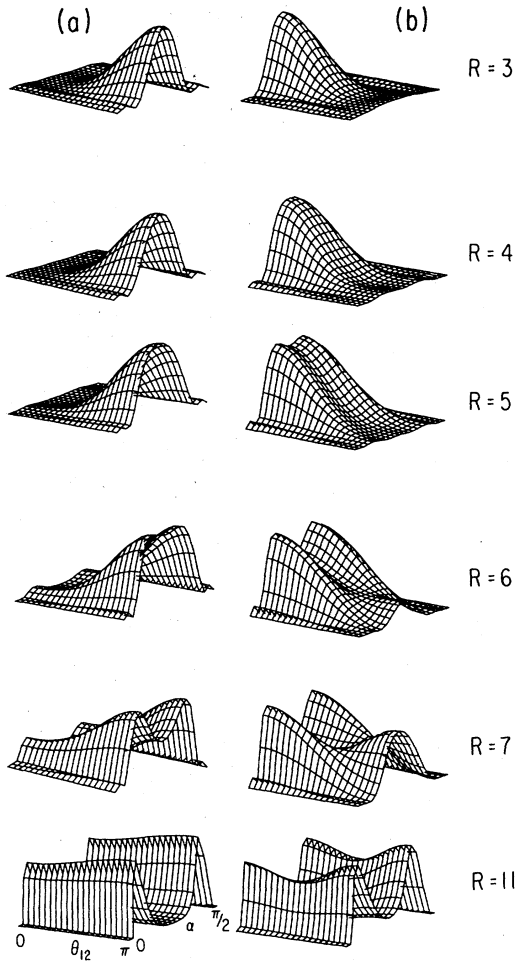


FIG. 2. Probability densities $\sigma_\mu(R;\alpha,\theta_{12})$ shown for different values of $R$: (a) the $\mu=1$ and (b) the $\mu=2$ adiabatic channels.

Figures 2(a) and 2(b) show the rotation-averaged probability density at several values of $R$, $\sigma_\mu(R;\alpha,\theta_{12})$ obtained by integrating over $\alpha',\theta_1',\phi_1',\theta_2',\phi_2'$ as follows:

$$\sigma_\mu(R;\alpha,\theta_{12})=\int d\Omega'\,\Phi_\mu(R;\Omega')\delta(\alpha'-\alpha)\times\delta(\cos\theta_{12}'-\cos\theta_{12})\Phi_\mu(R;\Omega)\ . \tag{8}$$

The radial and angular correlations of the two electrons can be visualized through these plots. At $R=4$, where $U_1(R)$ has its minimum, a high degree of radial and angular correlation between the two electrons is apparent as $\sigma_1$ peaks at $\theta_{12}=180°$ and $\alpha=\pi/4$, i.e., at opposite sides of the nucleus and with $r_1=r_2$. As we go through the crossing region, the radial and angular correlations begin to decrease and eventually at $R=11$ no evidence of radial or angular correlation is observed as one of the electrons remains bound in the $3s$ state of $Mg^+$ at $\alpha\sim 0$ or $\pi/2$. The other channel function, plotted in Fig. 2(b), shows the opposite behavior at low $R$, peaking at $\theta_{12}=0°$ and $\alpha=\pi/4$. An interesting phenomenon occurs at larger $R$

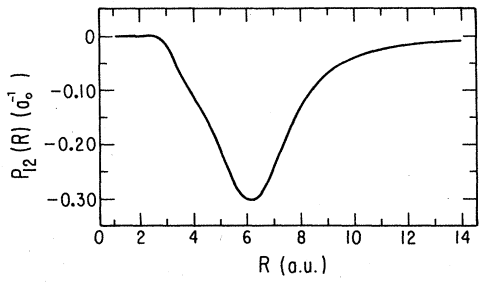


FIG. 3. Nonadiabatic coupling matrix element $P_{12}(R)$ between the two lowest adiabatic curves of Mg $^1D^e$.

in the vicinity of the crossing. At $R=7$, $\sigma_2$ has a peak at $\alpha=\pi/4$ and $\theta_{12}=180°$ showing the character present in the $\mu=1$ channel at low $R$. This demonstrates that, were the curves to cross, $U_1(R)$ would in fact converge to the $3p$ limit and $U_2(R)$ to the $3s$ limit.

The quantity $P_{12}(R)=\langle\Phi_1(R;\Omega)\,|\,\partial/\partial R\,|\,\Phi_2(R;\Omega)\rangle$, a measure of the breakdown of adiabaticity, is large when $\Phi_\mu(R;\Omega)$ changes rapidly with $R$. If, for example, $P_{12}(R)$ was zero for all $R$, the two adiabatic channels would be decoupled. Figure 3 shows a plot of this quantity as a function of $R$. It peaks at $R\approx 6.5$ where the crossing occurs and decays slowly at large $R$. This slow decay has caused numerical problems in evaluating scattering parameters. It is clear from the magnitude and width of $P_{12}(R)$ that nonadiabatic effects are important in this case. In Sec. II C we use an $R$-matrix procedure to evaluate these effects.

### C. MQDT parameters and quantum defects

We consider a finite volume $V$ outside of which the field is Coulombic and the solutions are known. We aim then at calculating the logarithmic derivative of the outgoing electron's wave function on the surface $S$ of the volume $V$. These solutions are then joined to Coulomb functions and the MQDT parameters are evaluated. This method is outlined in the following paragraphs.

Integrating by parts, Eq. (1) transforms into a variational expression for $b$, defined by

$$\frac{\partial\psi}{\partial n}+b\psi=0 \tag{9}$$

on the surface $S$ of the volume $V$, as follows:

$$b=\frac{\int_V[-(\nabla\psi^*)\cdot(\nabla\psi)+2\psi^*(E-U)\psi]dV}{\int_S\psi^*\psi dS}\,. \tag{10}$$

[For brevity $\nabla^2=\sum_{i=1}^2\nabla_i^2$, $U=V(r_1)+V(r_2)+1/r_{12}$.] (For details on the following procedure see Refs. 13 and 22.) On using a basis expansion of the form of Eq. (7) for $\psi(\mathbf{r}_1,\mathbf{r}_2)$ and extremizing (i.e., setting $\partial b/\partial C^{l_1 l_2}_{n_1 n_2}=0$), we obtain an eigenvalue problem for $b$,

$$\underline{\Gamma}\mathbf{C}=b\underline{\Lambda}\mathbf{C}\,, \tag{11}$$

where

$$\Gamma_{kl}=\int_V[-(\nabla y_k)\cdot(\nabla y_l)+2y_k(E-U)y_l]dV\,,$$
$$\Lambda_{kl}=\int_S y_k y_l dS \tag{12}$$

($y_k$ and $y_l$ represent the appropriate basis functions). The eigenvalues $b_\beta$ and their eigenvectors $\psi_\beta(\mathbf{r}_1,\mathbf{r}_2)$ provide us with the initial conditions for the outer electron's motion outside the ion's volume $V$. The electron moves in a Coulomb field outside $V$ where MQDT exploits the analytical properties of Coulomb functions and the usually slow energy dependence of their parameters.[15,16] Knowledge of eigenvalues $b_\beta$ and eigenvectors $\psi_\beta$ enables one to evaluate a $K$ matrix or an $S$ matrix. (The language of scattering theory is used throughout MQDT which rests on the concept of excitation channels.)

One goes over to the eigenchannel representation[16] in MQDT by transforming the $K$ matrix to its diagonal form, i.e., by constructing superpositions of the dissociation channels which diagonalize the reaction matrix. Diagonalizing $\underline{K}$ by a transformation $\underline{U}$,

$$\underline{U}^T\underline{K}\,\underline{U}=\tan(\pi\underline{\mu})\,, \tag{13}$$

we obtain its eigenvalues $\tan\pi\mu_\alpha$. An orthogonal transformation $\underline{U}$ for a two-channel system takes the form

$$\underline{U}=\begin{bmatrix}\cos\theta & \sin\theta\\ -\sin\theta & \cos\theta\end{bmatrix}\,, \tag{14}$$

the angle $\theta$ measuring the mixing between the $3s\epsilon d$ and $3p\epsilon p$ channels. $\mu_1$ and $\mu_2$ are the eigenquantum defects in each of the eigenchannels.

Figure 4(a) shows a plot of $\theta/\pi$ as a function of energy from an energy below the "$3s\,3d$" level to just above the $Mg^+(3p)$ threshold. $\mu_1$ and $\mu_2$ are plotted in the same energy range in Fig. 4(b). The first point of interest is the

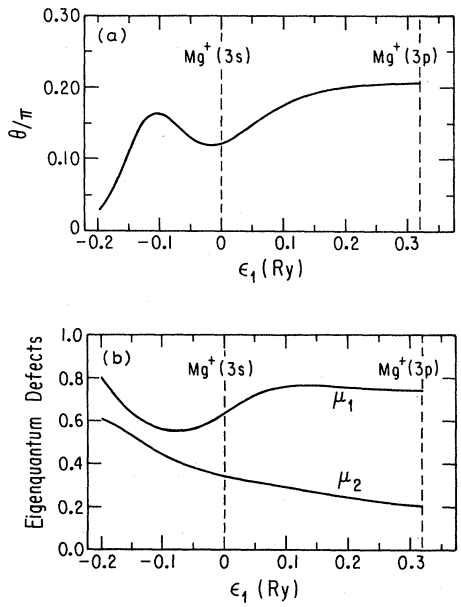


FIG. 4. MQDT parameters for Mg $^1D^e$ plotted as functions of the energy $\epsilon_1$ relative to the $Mg^+$ $3s$ threshold: (a) the mixing angle $\theta/\pi$ and (b) eigenquantum defects $\mu_1$ and $\mu_2$.

strong energy variation of the parameters in the energy range $-0.2<\epsilon_1<0.1$. The mixing angle rises from 0 to a values of about $\theta/\pi\approx 0.16$ at $\epsilon_1=-0.1$ and then dips as $\mu_1$ increases rapidly. The rise in $\mu_1$ reflects the penetration of the $d$ wave in the $3s\epsilon d$ channel into the reaction region, its amplitude therefore changing rapidly on the boundary. There is then an associated dip in $\theta/\pi$. A comprehensive measure of the channel interactions in this region is given by the scattering matrix element $S_{12}$ squared,[12]

$$|S_{12}|^2=\sin^2\pi(\mu_2-\mu_1)\sin^2(2\theta)\ . \tag{15}$$

At higher energies $\epsilon>0.1$, $|\mu_2-\mu_1|$ is $\approx 0.5$, $\theta/\pi$ approaches 0.25, and therefore $|S_{12}|^2\rightarrow 1.0$. The eigenchannels contain then roughly equal mixtures of the $3s\epsilon d$ and $3p\epsilon p$ channels. This circumstance has more general implications for the equipartition rule observed by Greene[12] in Be $^1P^o$ in that both radial and angular correlations are involved in this case. This is also the case for the heavier alkaline earths, Ca to Ra, where strong mixing is observed between the "$sp$" and "$pd$" channels.[23] We can study this mixing in more detail by examining the associated behavior of the helium doubly excited $^1D^e$ states converging to the $He^+(N=3)$ limit. Lin has recently examined these states.[9] He plots $\sigma_1(R;\alpha,\theta_{12})$ for the lowest adiabatic curve, labeled $(2,0)^+$ in the $(K,T)^A$ notation. His plot is identical to Fig. 2(a) at low $R$, however, at larger $R$ when the wave function begins to break into the $He^+$ $3s$ and $3p$ valleys, due to the rising potential barrier for double escape, the two electrons are no longer correlated radially but they maintain their angular correlation $\sigma_1(R;\alpha,\theta_{12})$ still peaking at $\theta_{12}=180°$. The degeneracy of the $3s$ and $3p$ levels in $He^+$ allows the angular correlation to persist to large distances. The $Mg^+$ $3s$ and $3p$ thresholds, on the other hand, are split by an energy $\Delta E\approx 0.3$ Ry and no angular correlation is apparent at $R=11$ in Fig. 2. However, we know from earlier studies of the $^1P^o$ states of Be and Mg that the partion of amplitude into the two dissociation channels occurs at a relatively low-value $R$ (at the avoided crossing at $R\approx 6.5$) where the splitting $\Delta E$ between the thresholds at large $R$ plays no role. Therefore for $\epsilon_1>0.1$ the only difference between the angular correlations in Mg and He at large $R$ will be due to the different amplitudes $F_1(R)$ and $F_2(R)$ of the radial wave functions for Mg in each of the adiabatic channels.

The quantum defects $\delta/\pi$ of the discrete levels and the phase shift $\delta$ in the continuum of each ionization channel can be calculated from the parameters $\mu_1$, $\mu_2$, and $\theta/\pi$, plotted in Fig. 4, as follows:[12]

$$\tan\delta=\frac{\sin(\pi\mu_1)\sin[\pi(\nu_2+\mu_2)]+\tan^2\theta\sin(\pi\mu_2)\sin[\pi(\nu_2+\mu_1)]}{\cos(\pi\mu_1)\sin[\pi(\nu_2+\mu_2)]+\tan^2\theta\cos(\pi\mu_2)\sin[\pi(\nu_2+\mu_1)]}\ , \tag{16}$$

where $\nu_2$ is given by $E-I_{3p}=-1/\nu_2^2$. Figure 5 shows $\delta/\pi$ as a function of energy. The "$3p^2$" cannot be identified in the spectrum, being distributed over the whole $3snd$ Rydberg series and the adjoining continuum. [There has been some controversy over the possible existence of the $3p^2$ level just below the $Mg^+(3s)$ threshold.[24,25] For completeness we have searched over a very fine energy mesh using the parameters shown in Fig. 4 and have found no evidence for such a level.] We obtain remarkably good agreement with experiment and with another more sophisticated calculation,[25] evidenced by Table I, even though we used Hartree-Slater potentials to represent the electron—closed-shell core interaction.

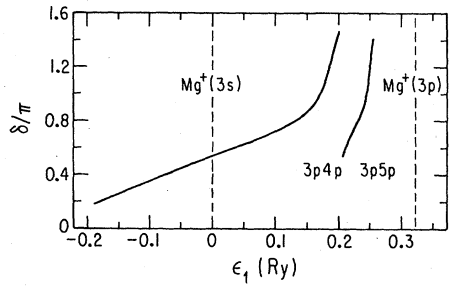


FIG. 5. $\delta/\pi$ vs $\epsilon_1$, the energy relative to the $Mg^+3s$ threshold. $\delta/\pi$ is equivalent to the quantum defect of the $3snd$ series for $\epsilon_1<0.0$ and it is shown here as a continuous function of energy. The quantum defects of the discrete levels shown in Table I are obtained by finding the intersection between this curve with $\delta/\pi=n-\nu_1$ where $\epsilon_1=-1/\nu_1^2$. The positions of the $3p4p$ and $3p5p$ autoionizing levels are indicated in the graph.

It is clear from the above analysis that the $sd$ and $p^2$ channels interact strongly. It should come as no surprise therefore, as pointed out in the Introduction, that the "$s^2d$"-"$sp^2$" interaction in Al I is also strong.

## III. ALUMINUM

As mentioned in the Introduction, there has been much interest in the Al $^2D^e$ spectrum because of the strong interaction between its $3s^2\epsilon d$ and $3s3pnp$ channels. Our work, in part, complements an earlier $R$-matrix study of the autoionizing levels above the $Al^+$ $^1S^e$ threshold carried out by Le Dourneuf *et al.*[5]

We used the $R$-matrix method outlined in Sec. II to calculate the MQDT parameters for the principal series in aluminum. This calculation is a step up in complexity compared to the calculations already performed in the al-

TABLE I. Magnesium $^1D^e$ quantum defects.

| Level | Experiment (Ref. 26) | Mendoza (Ref. 25) | This calculation |
|---|---|---|---|
| $3s3d$ | 0.3191 | 0.3111 | 0.3208 |
| $3s4d$ | 0.4146 | 0.4042 | 0.4231 |
| $3s5d$ | 0.4764 | 0.4639 | 0.4916 |
| $3s$ threshold | | | 0.5487 |

kaline earths. One reason for this is that $Al^+$ has two electrons outside a closed-shell core making it necessary to include electron correlation effects in evaluating the energy differences between its different thresholds. The $Mg^+$ and $Be^+$ ions, on the other hand, have a simple one-electron structure. Secondly, we are now dealing with a system of three interacting electrons and although the dominant interaction, as pointed out in Mg, is of the $sdp^2$ type, other configurations must be included to obtain satisfactory agreement with experiment.

The Hamiltonian for three electrons outside a closed-shell core, in a.u., is

$$H=\sum_{i=1}^{3}[-\tfrac{1}{2}\nabla_i^2+V(r_i)]+\sum_{i>j}\frac{1}{r_{ij}}\ , \tag{17}$$

where, as in the two-electron case, $V(r)$ represents the interaction between each of the electrons and the closed-shell core. The wave function $\psi(\mathbf{r}_1,\mathbf{r}_2,\mathbf{r}_3)$ is expanded in terms of antisymmetric basis functions within the reaction volume $V$ as before. This wave function, coupled to form a given total orbital angular momentum $\mathbf{L}$ and spin $\mathbf{S}$, is indicated symbolically as follows:

$$\psi=A\sum_{n_1l_1n_2l_2n_3l_3}C_{n_1n_2n_3}^{l_1l_2l_3}G_{n_1l_1}(r_1)F_{n_2l_2}(r_2)K_{n_3l_3}(r_3)\{[Y_{l_1m_1}(\theta_1,\phi_1)Y_{l_2m_2}(\theta_2,\phi_2)]^{L_{12}}Y_{l_3m_3}(\theta_3,\phi_3)\}^{L}$$
$$\times\{[\chi_{s_1m_1}(1)\chi_{s_2m_2}(2)]^{S_{12}}\chi_{s_3m_3}(3)\}^{S}\ . \tag{18}$$

We then construct (11) from (18). The coefficients $C$ and the eigenvalues $b_\beta$ are obtained by solving Eq. (11) at a chosen total energy $E$. Matching to a product of $Al^+$ and Coulomb wave functions on the surface $S$ gives us the $K$ matrix as before.

Initially we only included configurations of the type $3s^2nd$ and $3s\,3pnp\ ^2D^e$ in the expansion (18). This calculation demonstrated the basic effect, in that the $3s\,3pnp$ channel mixes strongly with $3s^2\epsilon d$ channel over a wide energy range. However, to obtain closer agreement with experiment, it was necessary to include other configurations in the expansion (18). An indication of the relevant configurations needed is obtained through a CI calculation of the energy levels of $Al^+$. Ten $3sns'$ and $3pnp'$ configurations were used to calculate the $^1S^e$ levels of $Al^+$. The $^3P^o$ and $^1P^o$ levels were calculated using the $3snp'$, $3pns'$, and $3pnd$ configurations. The orbitals are generated numerically in Hartree-Slater potentials. The energy differences between "$3s^2$" $^1S^e$ and the "$3s\,3p$" $^3P^o$ and $^1P^o$ levels are given in Table II. Good agreement with experiment is obtained.[26] These ionic states are projected onto the solutions $\psi_\beta(\mathbf{r}_1,\mathbf{r}_2,\mathbf{r}_3)$ of Eq. (11) on the surface $S$ to evaluate the escaping electron's amplitude in each dissociation channel and hence the $K$ matrix.

Table III shows all the configurations used in our full three-electron calculation. The primed notation indicates orbitals that are not necessarily orthogonal to the unprimed orbitals. Nonorthogonal orbitals enlarge the number of integrals but adds flexibility to our basis set. The $^1P^o$ threshold of $Al^+$ is 7.42 eV above the $^1S^e$ threshold and 2.77 eV above $^3P^o$, therefore channels converging to the $^1P^o$ are strongly closed at energies close to the $^1S^e$ threshold. We enforced this condition by ensuring that the $np'$ wave functions in the $3s\,3p\ ^1P^o\,np'$ channel had zero amplitude on the surface $S$. This enables us to analyze the $^2D^e$ spectrum in terms of the two channels $(3s^2)^1S^o\,\epsilon d$ and $(3s\,3p)^3P^o\,\epsilon p'$. The $K$ matrix was calculated as in Sec. II, and the mixing angle and eigenquantum defects $\theta/\pi$, and $\mu_1$ and $\mu_2$, respectively, are plotted in Fig. 6 in the vicinity of the $^1S^e$ threshold. The most striking aspect of Figs. 6(a) and 6(b) is the similarity between the energy dependence of these MQDT parameters and those of Mg $^1D^e$ plotted in Fig. 4. In particular we again see the rise in $\mu_1$ due to the penetration of the $d$ wave and the associated behavior of $\theta/\pi$ in the energy range $-0.15<\epsilon_1<0.0$. $\theta/\pi$ also rises to $\frac{1}{4}$ at $\epsilon_1\approx 0.2$ Ry. The quantum defects of the discrete spectrum and the phase shift of the continuum function in the autoionization region are calculated using these parameters and Eq. (16). Figure 7 shows the quantum defect of the $3s^2nd$ series as a function of energy and the phase shift of the $d$ wave in the continuum. The rise by one of $\delta/\pi$ at $\epsilon_1\approx 0.21$ is due to the $(3s\,3p)^3P^o\,4p$ autoionizing resonance. The $3s\,3p^2$ configuration is clearly distributed throughout the $3s^2nd$ series as seen by the slow rise in the quantum defect just below the $^1S^e$ threshold. We obtain satisfactory agreement with experiment[2(b)] and a significant improvement on previous theoretical calculations especially for high Rydberg states (see Table IV) considering we have used a Hartree-Slater potential to represent the electron—closed-shell core interaction. The quantum defects seem to be generally lower than the experimental ones by about 0.05,

TABLE II. The energy differences between the $Al^+$ thresholds in a.u.

| | Experiment (Ref. 26) | Le Dourneuf *et al.* (Ref. 5) | This calculation |
|---|---|---|---|
| $\Delta(^3P^o\text{-}^1S^e)$ | 0.1709 | 0.162 | 0.1646 |
| $\Delta(^1P^o\text{-}^1S^e)$ | 0.2727 | 0.2709 | 0.2741 |

TABLE III. $^2D^e$ channels used in this calculation.

| Configuration | No. of orbitals |
|---|---|
| $(3s\,3s')^1S^e\,nd$ | 10 |
| $(3p\,3p')^1S^e\,nd$ | 5 |
| $(3s\,3p)^3P^o\,np'$ | 8 |
| $(3s\,3p)^1P^o\,np'$ | 5 |
| $(3s\,3d)^1P^o\,np'$ | 2 |
| $(3p\,3p')^3P^e\,nd$ | 2 |

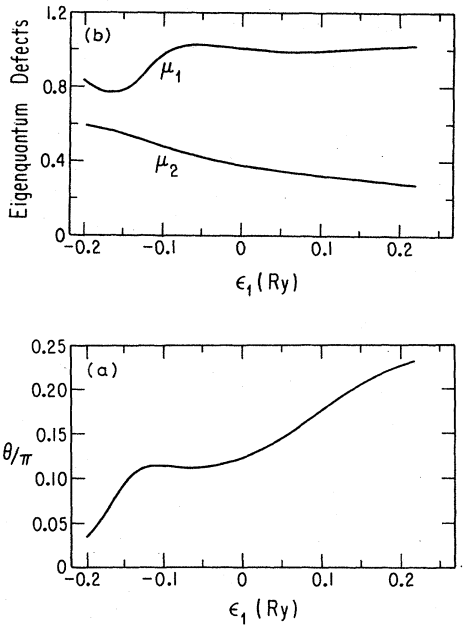


FIG. 6. MQDT parameters for Al $^2D^e$ plotted as functions of the energy $\epsilon_1$ relative to the $Al^+$ $^1S^e$ threshold. Shown are (a) the mixing angle $\theta/\pi$ and (b) the eigenquantum defects $\mu_1$ and $\mu_2$.

however, the profile of their rise agrees well with experiment as illustrated by the values in Table IV. As far as the evolution of electron correlations in Al is concerned we suspect that the three electrons "form" an equilateral triangle with the nucleus at its center in the low $R$ region, this being the generalization of the plus-type configuration for two electrons.[18] However, more work is required to detail the evolution of correlations for three-electron systems.

The $^2D^e$ series is, as we have seen, dominated by the interaction between the $3s^2\epsilon d$ and $3s\,3p\epsilon p$ channels. However, the $3s^2ns\ ^2S^e$ series interacts very weakly with the $3s\,3pnp\ ^2S^e$ channel. This is due in part to the Pauli exclusion principle which prevents the outer electron of the

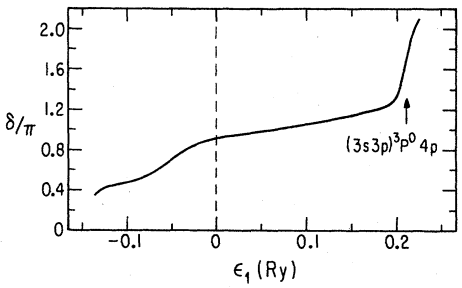


FIG. 7. $\delta/\pi$ vs the energy $\epsilon_1$ relative to the $Al^+$ $^1S^e$ threshold. The quantum defects $\mu \equiv \delta/\pi$ of the $3s^2nd$ series in the discrete region are drawn as a continuous function of energy. Note the rise in the quantum defect from about 0.4 to 1.0 below the $^1S^e$ threshold. This is due to the "$3s\,3p^2$" perturber. The position of the $(3s\,3p)^3P^o\,4p$ autoionizing level is also indicated.

TABLE IV. Aluminum $^2D^e$ quantum defects.

| Level | Experiment [Ref. 2(b)] | This calculation | Ref. 4 |
|---|---|---|---|
| $3s^23d$ | 0.3684 | 0.321 | 0.335 |
| $3s^24d$ | 0.5740 | 0.544 | 0.512 |
| $3s^25d$ | 0.7360 | 0.672 | 0.606 |
| $3s^26d$ | 0.8291 | 0.767 | 0.577 |
| $3s^27d$ | 0.8915 | 0.832 | 0.406 |
| $3s^28d$ | 0.9125 | 0.871 | |
| $^1S^e$ threshold | | 0.924 | |

$3s^2ns$ configurations from penetrating the valence shell, thus reducing the probability of excitation of the $3s\,3p^2$. This difference between alternate excitation channels is familiar from the noble gases Ar, Kr, and Xe, where the $nd$ autoionizing levels converging to the $p_{1/2}$ threshold have much larger widths than the $ns$ levels.[27] Neon, on the other hand, has a $2p^6$ core and the first $d$-wave excitation is to the $n=3$ shell. The $ns$ levels in this case have larger widths than the $nd$.[28]

## IV. DISCUSSION

The study of atomic excitations should be generally advanced by the methods described in this paper, namely, (1) the identification of critical regions of space and energy where channel excitation occurs, through such plots as Figs. 1 and 3, (2) the description of the motion of many-electron system by an analysis of its wave functions in configuration space (e.g., Fig. 2), and (3) the *ab initio* evaluation of channel-coupling effects through the calculation of a small set of MQDT parameters. We have illustrated particularly how these methods provide a clearer understanding of the $sd$-$p^2$ interaction in magnesium $^1D^e$ and of the analogous $s^2d$-$sp^2$ interaction in aluminum $^2D^e$. We are also able to calculate reliable energy levels in the discrete and phase shifts in the autoionizing and continuum regions. These calculations required *little computational effort* in that, for example, the whole aluminum calculation, from the generation of the basis set to the calculation of the MQDT parameters and quantum defects at all energies, took 30 CPU (central processing unit) seconds on an IBM 3081 computer or about five minutes on a Digital Equipment Corporation VAX 11/780. This section outlines how our analysis can be brought to bear on some outstanding problems.

Calculations on the heavier alkaline earths Ca, Sr, and Ba are desirable as there exist extensive experimental data, particularly in barium.[29] The nature of the $\pm$ equipartition rule observed in calculations on the $^1P^o$ states of Be and Mg also needs to be investigated for these heavier atoms. However it will not be possible to represent the electron—closed-shell core interaction by a Hartree-Slater potential, as was done in this paper, due to the sensitivity of, for instance, the $3d$ wave function in $Ca^+(3d)$ to this interaction. A local-density approximation of the kind used by Armstrong *et al.*[30] might suffice for this purpose. Spin-orbit coupling effects should also be included in calculations, at least for barium. Extensive data exists also

on the excitation of the resonance line of the alkali metals by low-energy electron impact, collected mainly by Gallagher's group.[31] An analysis of such data may prove particularly interesting in that fairly elaborate close-coupling calculations have only come within 10% of the experimental excitation cross section for the analogous $2s$ to $2p$ transition in electron-$Be^+$.[32]

Our work on aluminum should be readily generalizable to the other group-III elements Ga, In, and Tl. Synchrotron radiation measurements on the "$nsnp(n+1)p$" autoionizing resonances of these atoms have been performed recently.[33] Scott, Burke, and Bartschat[34] have used a Hamiltonian of the form of Eq. (17) plus spin-orbit coupling terms in their analysis of low-energy inelastic electron scattering on Hg. Electron-Cs scattering and electron—spin-polarization effects in these atoms were also studied.[35] Further elucidation of the evolution of correlations in three-electron systems through plots of the type shown in Fig. 2 or by some other means is desirable.

As mentioned earlier, aspects of the silicon spectrum initiated this work. The $^3P^o$ and $^3D^o$ "$3s^2spnd$" spectra are perturbed by the $3s\,3p^3$ configuration.[36] An attempt to fit the $^3P^o$ series by Mies's[37] quantum-defect treatment of the effect of an isolated perturber on a Rydberg series yielded fairly poor results. This shortcoming is now understandable in view of our Al and Mg calculations, in that the strong energy dependence of the MQDT parameters due to electron correlations makes Mies's simple treatment unrealistic in this case. There exists a wealth of detailed spectroscopic data on the group-IV elements on which *ab initio* calculations remain to be done.[36]

## ACKNOWLEDGMENTS

I would like to than Professor U. Fano for his direction and support throughout this work and for his assistance with the manuscript. I appreciate the help given to me by Dr. S. Watanabe, Dr. M. Le Dourneuf, and Dr. J. M. Launay of the Observatoire de Paris, Meudon, where some of this work was carried out. I have also benefitted from interactions with Dr. C. H. Greene, Dr. K. T. Cheng, and Dr. C. D. Lin. I would like to thank J. Tan for her assistance in the analysis of the strong perturbations of the silicon spectrum. This work was supported by the Office of Basic Energy Sciences of the U.S. Department of Energy and partly by the Centre National de la Recherche Scientifique—National Science Foundation (CNRS—NSF), France—United States cooperative science program, and by NATO under Contract No. 328. It was presented as a thesis to the Department of Physics, The University of Chicago, in partial fulfillment of the requirements for the Ph.D. degree.

---

*Present address: Department of Mathematics, Royal Holloway and Bedford College, University of London, Egham Hill, Egham, Surrey TW20 0EX, Surrey, United Kingdom.

[1]C. D. Lin, Astrophys. J. **187**, 385 (1974).
[2](a) N. P. Penkin and L. N. Shabanova, Opt. Spectrosc. **18**, 504 (1965); (b) K. B. S. Eriksson and H. B. S. Isberg, Ark. Fys. **23**, 527 (1962).
[3]A. W. Weiss, Phys. Rev. **178**, 82 (1969).
[4]A. W. Weiss, Phys. Rev. A **9**, 1524 (1974).
[5]M. Le Dourneuf, Vo Ky Lan, P. G. Burke, and K. T. Taylor, J. Phys. B **8**, 2640 (1975).
[6]U. Fano, Phys. Rev. A **24**, 2402 (1981).
[7]M. J. Cavagnero, Phys. Rev. A **30**, 1169 (1984).
[8]J. W. Cooper, U. Fano, and F. Prats, Phys. Rev. Lett. **10**, 518 (1963).
[9]C. D. Lin, Phys. Rev. A **29**, 1019 (1984).
[10]D. R. Herrick and O. Sinanoğlu, Phys. Rev. A **11**, 97 (1975).
[11]D. R. Herrick and M. E. Kellman, Phys. Rev. A **21**, 418 (1980); D. R. Herrick, M. E. Kellman, and R. D. Pollak, *ibid.* **22**, 1517 (1980).
[12]C. H. Greene, Phys. Rev. A **23**, 661 (1981).
[13]P. F. O'Mahony and C. H. Greene, Phys. Rev. A **31**, 250 (1985).
[14]P. F. O'Mahony and S. W. Watanabe, J. Phys. B **18**, L239 (1985).
[15]For a recent review of MQDT, see M. J. Seaton, Rep. Prog. Phys. **46**, 167 (1983).
[16]K. T. Lu, Phys. Rev. A **4**, 579 (1971); C. M. Lee and K. T. Lu, *ibid.* **8**, 1241 (1973), and references therein.
[17]C. H. Greene and C. W. Clark, Phys. Rev. A **30**, 2161 (1984).
[18]S. Watanabe, M. Le Dourneuf, and L. Pelamourgues, Colloque International 334 du C.N.R.S [J. Phys. (Paris) Colloq. **43**, CX-223 (1982)].
[19]J. P. Desclaux, Comput. Phys. Commun. **1**, 216 (1969).
[20]J. H. Macek, J. Phys. B **1**, 831 (1968); for a review of the hyperspherical method, see U. Fano, Rep. Prog. Phys. **46**, 97 (1983).
[21]C. D. Lin, Phys. Rev. A **23**, 1585 (1981).
[22]C. H. Greene, Phys. Rev. A **28**, 2209 (1983); see also H. Le Rouzo and G. Raseev, *ibid.* **29**, 1214 (1984).
[23]J. A. Armstrong, J. J. Wynne, and P. Esherick, J. Opt. Soc. Am. **69**, 211 (1979).
[24]D. J. Bradley, P. Ewart, J. V. Nicholas, J. R. D. Shaw, and D. G. Thompson, Phys. Rev. Lett. **31**, 273 (1973).
[25]C. Mendoza, J. Phys. B **14**, 397 (1981).
[26]C. E. Moore, *Atomic Energy Levels,* Natl. Bur. Stand. Ref. Data Ser., Natl. Bur. Stand (U.S.) Circ. No. 467 (U.S. GPO, Washington, D.C., 1949), Vols. I—III.
[27]W. R. Johnson, K. T. Cheng, K. N. Huang, and M. Le Dourneuf, Phys. Rev. A **22**, 989 (1980).
[28]W. R. Johnson and M. Le Dourneuf, J. Phys. B **13**, L13 (1980).
[29]For a recent review of both experiment and theory, see M. Aymar, Phys. Rep. **110**, 163 (1984).
[30]J. A. Armstrong, S. S. Jha, and K. C. Pandey, Phys. Rev. A **23**, 2761 (1981); K. C. Pandey, S. S. Jha, and J. A. Armstrong, Phys. Rev. Lett. **44**, 1583 (1980).
[31]S. T. Chen and A. C. Gallagher, Phys. Rev. A **17**, 551 (1978), and references therein; B. Jaduszliwer, P. Weiss, A. Tino, and B. Bederson, *ibid.* **30**, 1255 (1984).
[32]M. A. Hayes, D. W. Norcross, J. B. Mann, and W. D. Robb, J. Phys. B **10**, L429 (1977).
[33]J. P. Connerade and M. A. Baig, J. Phys. B **15**, L587 (1982).
[34]N. S. Scott, P. G. Burke, and K. Bartschat, J. Phys. B **16**,

L361 (1983).
[35]N. S. Scott, K. Bartschat, P. G. Burke, O. Nagy, and W. B. Eissner, J. Phys. B **17**, 3755 (1984).
[36]C. M. Brown, S. G. Tilford, R. Tousey, and M. L. Ginter, J. Opt. Soc. Am. **64**, 1665 (1974); C. M. Brown, S. G. Tilford, and M. L. Ginter, *ibid.* **67**, 1240 (1977), and references therein.
[37]F. H. Mies, Phys. Rev. A **20**, 1773 (1979).